



Uncorrelated Amplitude and Frequency Variations of the Harmonics in SX Phoenicis Star XX Cygni

Jia-Shu Niu (牛家树)^{1,2} , Yue Liu (刘越)¹, and Hui-Fang Xue (薛会芳)^{3,4}

¹ Institute of Theoretical Physics, Shanxi University, Taiyuan 030006, People's Republic of China; jsniu@sxu.edu.cn, hfxue@tynu.edu.cn

² State Key Laboratory of Quantum Optics and Quantum Optics Devices, Shanxi University, Taiyuan 030006, People's Republic of China

³ Department of Physics, Taiyuan Normal University, Jinzhong 030619, People's Republic of China

⁴ Institute of Computational and Applied Physics, Taiyuan Normal University, Jinzhong 030619, People's Republic of China

Received 2023 May 1; accepted 2023 May 29; published 2023 July 4

Abstract

Harmonics are quite common in pulsating stars. They are always considered to mimic the behaviors of their independent parent pulsation modes, and are not taken for key information in asteroseismology. Here, we report an SX Phoenicis star XX Cygni, whose periodogram is dominated by the fundamental frequency $f_0 = 7.41481 \pm 0.00004$ c day⁻¹ and its 19 harmonics. According to the analysis of the archival data from the Transiting Exoplanet Survey Satellite (TESS), we find that both the amplitudes and frequencies of the fundamental mode and the harmonics vary within TESS Sectors 14–17 and 54–57, which might be caused by the contamination of neighboring stars. What is more interesting is that the harmonics show significantly uncorrelated amplitude and frequency variations over time. Some possible origins and interesting issues are proposed to scheme further research of this hidden corner in current asteroseismology.

Unified Astronomy Thesaurus concepts: Pulsating variable stars (1307); Stellar pulsations (1625); SX Phoenicis variable stars (1673)

1. Introduction

Harmonics are usually accompanied by the independent pulsation modes among pulsating stars, such as Cepheids (Rathour et al. 2021), RR Lyrae stars (Kurtz et al. 2016), δ Scuti stars (Breger & Montgomery 2014), high-amplitude δ Scuti stars (Niu et al. 2017), SX Phoenicis stars (Xue & Niu 2020), γ Dor stars (Kurtz et al. 2015), pulsating white dwarfs (Wu 2001), β Cep stars (Degroote et al. 2009), and SPB stars (Pápics et al. 2017). It is generally believed that the harmonics come from the nonsinusoidal nature of light curves, which indicates the nonlinearity of the star's pulsation. Such as the nonlinear transformation from the temperature variation to the flux variation ($F = \sigma T^4$), and the nonlinear feedback of the stellar medium to the pulsation waves. As a result, the harmonics are not considered as the intrinsic stellar pulsation modes (Brickhill 1992; Wu 2001) and should mimic the behaviors of the parent pulsation modes. In practice, the harmonics are always removed in the prewhitening process and not taken as key information for asteroseismology.

δ Scuti stars are a class of short-period pulsating variable stars with periods between 15 minutes and 8 hr and the spectral classes A–F, which are located on the main-sequence or post-main-sequence evolutionary stage at the bottom of the classical Cepheid instability strip, and are self excited by the κ mechanism (Breger 2000; Handler 2009; Uytterhoeven et al. 2011; Holdsworth et al. 2014). High-amplitude δ -Scuti stars (hereafter HADS) are a subclass of δ -Scuti stars, which always have larger amplitudes and slower rotations. Most of the HADS show single or double radial-pulsation modes (Niu et al. 2013, 2017; Xue et al. 2018; Alton 2019; Bowman et al. 2021; Alton 2022a, 2022b; Daszyńska-Daszkiewicz et al. 2022), and some of them have three

radial-pulsation modes (Handler et al. 1998; Wils et al. 2008; Mow et al. 2016; Yang et al. 2021; Poleski et al. 2010; Khruslov 2014; Kazarovets et al. 2020; Khruslov 2022; Niu & Xue 2022), or even some nonradial pulsation modes (Poretti et al. 2011). SX Phoenicis (SX Phe) stars, a subgroup of HADS, are old Population II stars, which are characterized by high amplitudes of pulsation, low metallicity, and large spatial motion.

XX Cygni (hereafter XX Cyg, $\alpha_{2000} = 20^{\text{h}}03^{\text{m}}16^{\text{s}}$, $\delta_{2000} = 58^{\circ}57'17''$, $V = 11.86$ mag) is an Population II SX Phe star pulsating with a single radial mode (Cerasiki 1904; Nijland 1923; McNamara & Feltz 1980; Szeidl & Mahdy 1981; Joner 1982; Hintz & Joner 1997; Kiss & Derekas 2000; Zhou et al. 2002; Blake et al. 2003), which shows a continuous linear-period variation rate of $(1/P_0)(dP_0/dt) = 1.19(13) \times 10^{-8}$ yr⁻¹ (Yang et al. 2012). Although XX Cyg has a clean periodogram (which consists of the fundamental frequency $f_0 = 7.4148$ c day⁻¹ and its harmonics), the residuals in the $O - C$ diagram have deviations of about 0.001–0.005 day, which is an order of magnitude larger than the uncertainties of the times of maximum light (TML; about 0.0001 day). These dispersions in the residuals indicate that the apparently stable single pulsation mode is actually not that stable.

These years, XX Cyg has been monitored by the Transiting Exoplanet Survey Satellite (TESS; Ricker et al. 2015), whose continues photometric data provide us an opportunity to study the stability of the pulsation mode in detail. In the case of single-mode pulsator like XX Cyg, the instability of the pulsation mode can be reflected by the variations of the amplitudes and frequencies of the fundamental mode and its harmonics.

2. Methods

XX Cyg (TIC 233310793) has been observed by TESS spacecraft continuously during Sectors 14–17 in 2019 (BJD 2458683–2458788; Data Set 1; DS1) and Sectors 54–57 in 2022 (BJD 2459770–2459882, Data Set 2; DS2), whose



Original content from this work may be used under the terms of the [Creative Commons Attribution 4.0 licence](#). Any further distribution of this work must maintain attribution to the author(s) and the title of the work, journal citation and DOI.

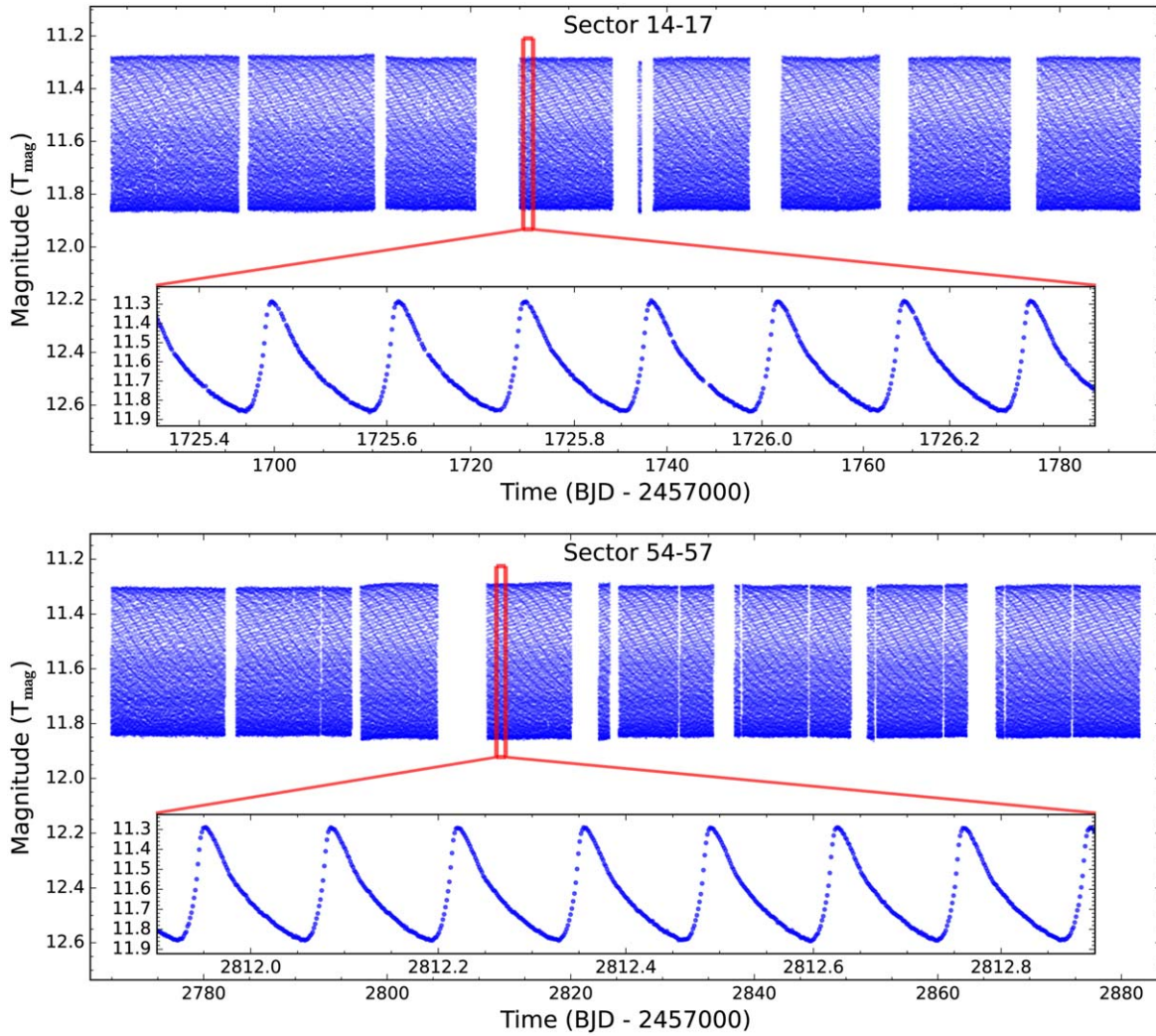


Figure 1. Light curves of XX Cyg observed by TESS.

photometric data has gaps of about 3–4 days in the same Sector and between the continuous Sectors (see in Figure 1).⁵ We downloaded the 2 minute cadence flux measurements, which were processed by the TESS Science Processing Operations Center (Jenkins et al. 2016) from the MAST Portal.⁶ After converting the normalized fluxes to magnitudes by utilizing the TESS magnitude of +11.6412 and removing the long trends in each Sectors, we totally got 127055 data points (DS1+DS2). The light curves are shown in Figure 1.

In Figure 2, the Fourier analysis was performed on DS2 to present the periodogram of XX Cyg,⁷ in which we marked $f_0 = 7.41481 \pm 0.00004 \text{ c day}^{-1}$ and its 19 harmonics. The detailed information of them are listed in Table 1.

In order to extract the variation information in the amplitudes and frequencies over time, we used the short-time Fourier transformation to deal with the light curves of DS1 and DS2 separately (see, e.g., Niu & Xue 2022 for more details). The prewhitening process in a time window of 30 days was

performed when the window was moving from the start to the end time of the data set, with a step of 3 days. In each step in the prewhitening process, the Lomb–Scargle algorithm (VanderPlas 2018) was used to help find the initial value of frequency with the largest amplitude, and then a nonlinear least-square fitting was performed to get the final values of the frequency, amplitude, and phase (Niu & Xue 2022). At last, the fundamental pulsation mode (labeled as F0) and its 19 harmonics (labeled as F1 to F19) were considered in this work due to the signal-to-noise ratio of them in most of the moving time windows. The amplitudes and frequencies of F0 to F19 over time are shown in Figures 3 and 4.

In this work, the uncertainties of amplitudes (σ_a) are defined as the median value of the amplitudes within a spectral window of 4 c day^{-1} equally divided by the frequency peak (similar to that in Zong et al. 2018; Niu & Xue 2022), while the uncertainties of the frequencies (σ_f) are estimated following relationship between the amplitude and frequency proposed by Montgomery & Odonoghue (1999) and Aerts (2021),

$$\sigma_f = \sigma_a \cdot \frac{\sqrt{3}}{\pi \cdot A \cdot T}, \quad (1)$$

⁵ XX Cyg has also been observed by TESS in Sector 41 in 2021 (BJD 2459420–2459447), which is not used in this work because of the short duration of the data.

⁶ <https://mast.stsci.edu/portal/Mashup/Clients/Mast/Portal.html>

⁷ It is because that DS2 has more data points and a longer baseline compared with DS1.

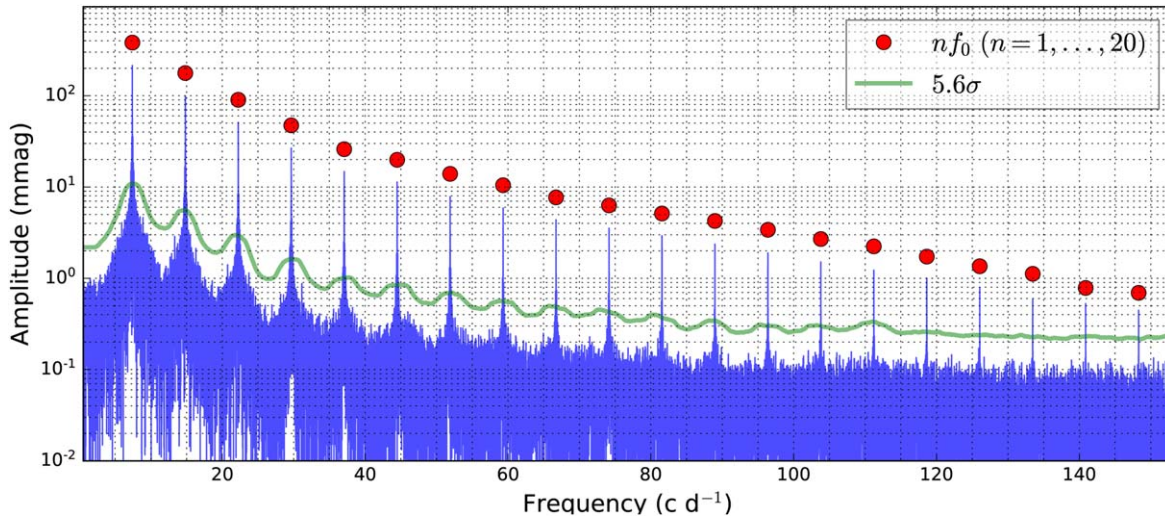


Figure 2. Periodogram of XX Cyg based on DS2. The fundamental frequency and its harmonics are marked as the red dots.

Table 1
Multifrequency Solution of the TESS Light Curves of XX Cyg Based on DS2

| ID | Marks | Frequency (c day^{-1}) | σ_f (c day^{-1}) | Amplitude (mmag) | σ_a (mmag) | S/N |
|-----|---------|-----------------------------------|------------------------------------|------------------|-------------------|-------|
| F0 | f_0 | 7.41481 | 0.00004 | 214.20 | 1.94 | 110.6 |
| F1 | $2f_0$ | 14.82961 | 0.00004 | 99.68 | 0.88 | 112.8 |
| F2 | $3f_0$ | 22.24446 | 0.00004 | 50.97 | 0.45 | 112.2 |
| F3 | $4f_0$ | 29.65926 | 0.00004 | 26.75 | 0.24 | 110.8 |
| F4 | $5f_0$ | 37.07406 | 0.00004 | 14.73 | 0.13 | 109.3 |
| F5 | $6f_0$ | 44.48886 | 0.00005 | 11.23 | 0.10 | 107.8 |
| F6 | $7f_0$ | 51.90371 | 0.00004 | 7.89 | 0.07 | 110.2 |
| F7 | $8f_0$ | 59.31851 | 0.00005 | 5.90 | 0.06 | 103.9 |
| F8 | $9f_0$ | 66.73327 | 0.00005 | 4.41 | 0.04 | 98.3 |
| F9 | $10f_0$ | 74.14811 | 0.00005 | 3.59 | 0.04 | 89.6 |
| F10 | $11f_0$ | 81.56296 | 0.00006 | 2.94 | 0.03 | 86.8 |
| F11 | $12f_0$ | 88.97771 | 0.00006 | 2.39 | 0.03 | 78.1 |
| F12 | $13f_0$ | 96.39256 | 0.00007 | 1.94 | 0.03 | 70.7 |
| F13 | $14f_0$ | 103.80741 | 0.00008 | 1.55 | 0.03 | 61.2 |
| F14 | $15f_0$ | 111.22216 | 0.00009 | 1.25 | 0.02 | 52.8 |
| F15 | $16f_0$ | 118.6372 | 0.0001 | 1.01 | 0.02 | 45.1 |
| F16 | $17f_0$ | 126.0519 | 0.0001 | 0.78 | 0.02 | 38.1 |
| F17 | $18f_0$ | 133.4666 | 0.0002 | 0.60 | 0.02 | 30.2 |
| F18 | $19f_0$ | 140.8813 | 0.0002 | 0.46 | 0.02 | 24.0 |
| F19 | $20f_0$ | 148.2962 | 0.0003 | 0.34 | 0.02 | 18.6 |

Note. σ_f denotes the error estimation of frequency, σ_a denotes the error estimation of amplitude. S/N is calculated within a spectral window of 4 c day^{-1} equally divided by the frequency peak.

3. Results

In Figure 3, it is clear that the amplitudes in DS1 are systematically greater than that in DS2 from F0 to F14, which might be caused by the contamination by neighboring stars. As the order of the harmonics increases (from F15 to F19), it seems not that obvious and shows more fluctuations. In Figure 4, it shows that the frequencies are stable within the uncertainties for the fundamental mode and first several harmonics (from F0 to F9), and the situations become complex and more fluctuations emerge as the order of the harmonic increases.

What is more interesting is that the different harmonics show uncorrelated variations both in amplitude and frequency, which is almost impossible to be affected by the contamination by neighboring stars. For example, the amplitude of F16 increases

after 1720 (BJD-2457000), while that of F19 decreases after that time. Meanwhile, the frequency of F16 shows two bumps at about 1710 and 1740 (BJD-2457000), while that of F19 shows only one bump at about 1740 (BJD-2457000).

In order to show the uncorrelated variations of the amplitude and frequency of the fundamental pulsation mode and its harmonics, their amplitudes and frequencies are renormalized as $A_i \equiv A_i / \langle A_i \rangle$ and $f_i \equiv f_i / \langle f_i \rangle$, where $\langle A_i \rangle$ and $\langle f_i \rangle$ denote the time-averaged values of the amplitude A_i and frequency f_i of F_i . Meanwhile, the uncertainties of A_i and f_i are obtained by $\sigma_{A_i} \equiv \sigma_{A_i} / \langle A_i \rangle$ and $\sigma_{f_i} \equiv \sigma_{f_i} / \langle f_i \rangle$, where σ_{A_i} and σ_{f_i} are the uncertainties of the amplitude and frequency of F_i . The time-averaged normalized amplitude and frequency uncertainties of F0 to F19 ($\langle \sigma_{A_i} \rangle$ and $\langle \sigma_{f_i} \rangle$) are listed in Table 2.

In order to show the uncorrelated variations of the amplitude and frequency clearly, we choose the amplitudes of F1 (A_1)

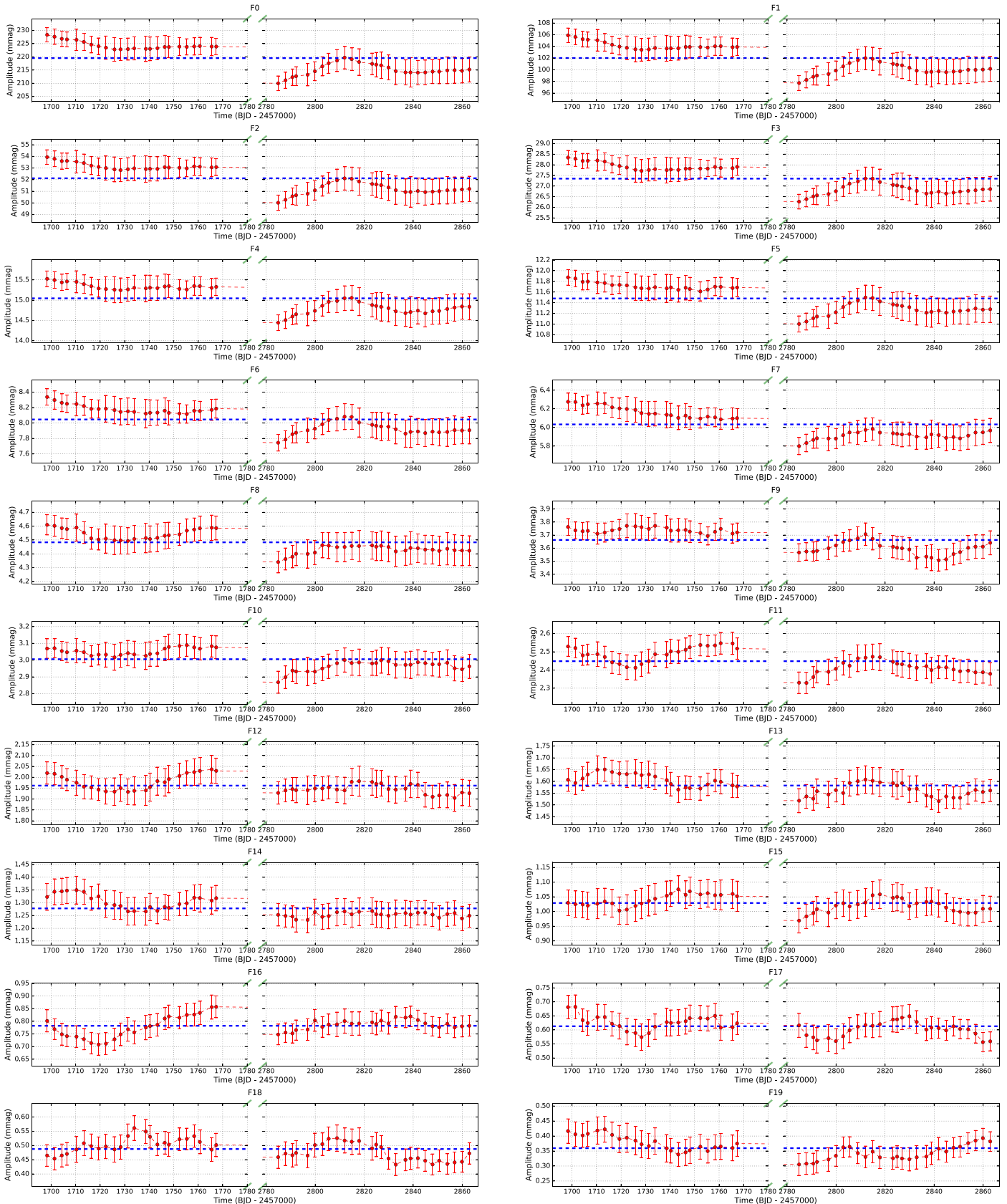


Figure 3. Variations of the amplitudes of F0 to F19. The red dots with errorbars present the amplitudes in moving windows, and the blue dashed lines present the time-averaged amplitudes.

and the frequencies of F11 (f11) as the bases to present the correlation chart (A_i versus A_1 and f_i versus f_{11}) in Figures 5 and 6, which have the smallest time-averaged uncertainties.

In Figures 5 and 6, we treat the points in each of the subfigures obeying the two-dimensional normal distributions $N(A_i, A_1, \sigma_{A_i}, \sigma_{A_1}, 0)$ and $N(f_i, f_{11}, \sigma_{f_i}, \sigma_{f_{11}}, 0)$. If the points

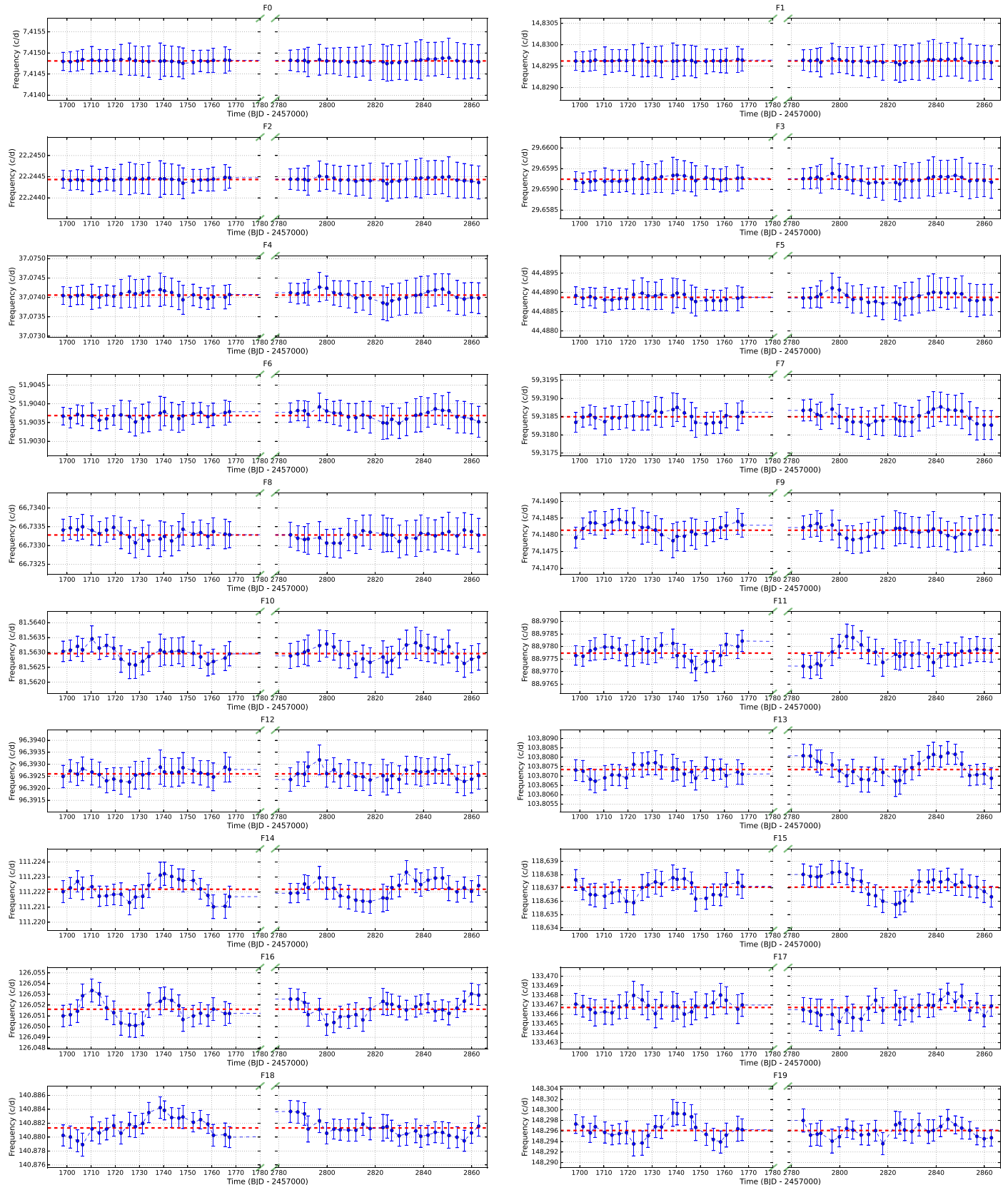


Figure 4. Variations of the frequencies of F0 to F19. The blue dots with errorbars present the frequencies in moving windows, and the red dashed lines present the time-averaged frequencies.

deviate the diagonals more than 1σ , we plot them with dark red/blue dots (with errorbars) rather than light ones, which helps us to find the significantly deviated points clearly.

For the amplitudes, as the order of the harmonic increases, the tendency to deviate from the diagonals is growing stronger. From A16 to A19, it is clear that some points deviate the

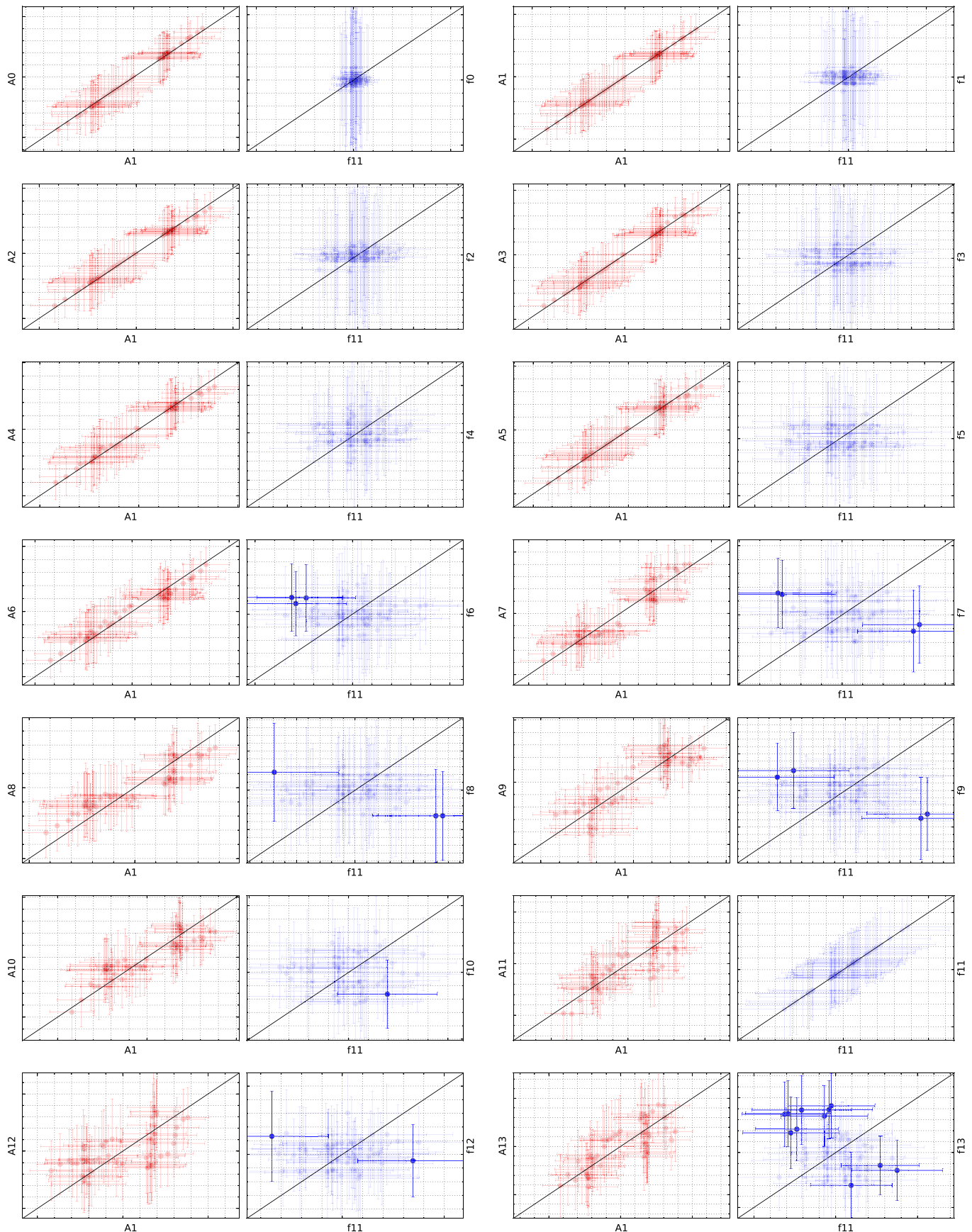


Figure 5. Correlation chart based on F1 (amplitude) and F11 (frequency), Part I.

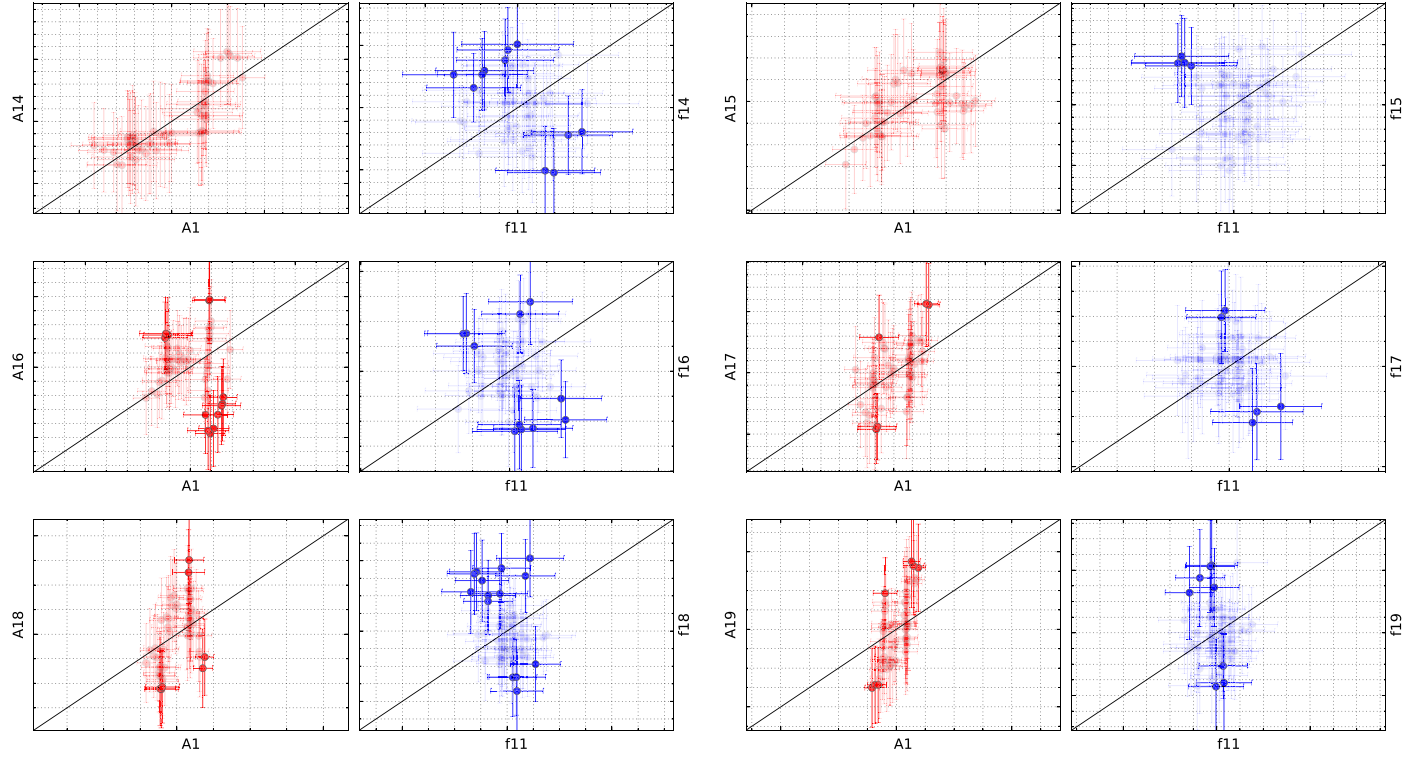


Figure 6. Correlation chart based on F1 (amplitude) and F11 (frequency), Part II.

diagonal significantly, which indicates that the amplitudes of F16 to F19 show uncorrelated variations comparing with F1. For the frequency, we cannot find the significantly deviated points from F0 to F5 because of the relatively large uncertainties of σ_{fi} ($i = 0, 1, 2, 3, 4, 5$), although it shows uncorrelated variation tendency with F11. However, from F6 to F19 (except F11 itself), we can confirm that some points deviate the diagonals significantly, which indicates that the frequencies of F6 to F19 show uncorrelated variations comparing with F11. Consequently, both the amplitudes and frequencies of the harmonics show uncorrelated variations, which is a challenge to our common perception that the harmonics should mimic the behaviors of their parent pulsation mode. There must be some unrevealed mechanisms hidden inside.

4. Discussions and Conclusions

In history, the period/frequency variation of the dominating pulsation mode of some kinds of pulsating stars can be obtained via the accumulation of the TML lasts for several decades by $O - C$ method (such as Cepheid; Csörnyei et al. 2022; Yacob et al. 2022; RR Lyrae stars; Li et al. 2018; HADS; Xue et al. 2022; and SX Phe stars; Xue & Niu 2020). An interesting but often overlooked detail is that it always exists dispersions in the $O - C$ diagrams, which are always one or more orders of magnitude larger than the TML uncertainties (Li et al. 2018; Xue & Niu 2020; Csörnyei et al. 2022; Xue et al. 2022; Yacob et al. 2022). This phenomenon not only happens for multimode pulsating stars, but also for the single-mode ones. In the former case, we can ascribe it to the perturbations from the nondominating pulsation modes to the dominating one. However, in the latter case, the $O - C$ dispersions (about 0.001–0.005 day for XX Cyg; see Figure 6 of Yang et al. 2012) should not exceed the level of TML uncertainties (about

Table 2
Time-averaged Uncertainties of A_i and f_i

| ID | $\langle \sigma_{Ai} \rangle$ | $\langle \sigma_{fi} \rangle$ |
|-----|-------------------------------|-------------------------------|
| F0 | 1.83×10^{-2} | 4.65×10^{-5} |
| F1 | 1.81×10^{-2} | 2.31×10^{-5} |
| F2 | 1.82×10^{-2} | 1.54×10^{-5} |
| F3 | 1.83×10^{-2} | 1.17×10^{-5} |
| F4 | 1.86×10^{-2} | 9.44×10^{-6} |
| F5 | 1.88×10^{-2} | 7.96×10^{-6} |
| F6 | 1.90×10^{-2} | 6.89×10^{-6} |
| F7 | 1.98×10^{-2} | 6.29×10^{-6} |
| F8 | 2.12×10^{-2} | 5.99×10^{-6} |
| F9 | 2.23×10^{-2} | 5.67×10^{-6} |
| F10 | 2.38×10^{-2} | 5.49×10^{-6} |
| F11 | 2.59×10^{-2} | 5.48×10^{-6} |
| F12 | 2.99×10^{-2} | 5.83×10^{-6} |
| F13 | 3.29×10^{-2} | 5.95×10^{-6} |
| F14 | 3.91×10^{-2} | 6.62×10^{-6} |
| F15 | 4.54×10^{-2} | 7.20×10^{-6} |
| F16 | 5.46×10^{-2} | 8.15×10^{-6} |
| F17 | 6.97×10^{-2} | 9.84×10^{-6} |
| F18 | 8.30×10^{-2} | 1.11×10^{-5} |
| F19 | 1.09×10^{-1} | 1.39×10^{-5} |

0.0001 day for XX Cyg; see Table 3 of Yang et al. 2012) too much, unless the apparently stable pulsation mode is actually not stable.

As that has been revealed in this work, the $O - C$ dispersions in these single-mode pulsating stars can also be represented by the uncorrelated amplitude and frequency variations of the harmonics. As a result, the uncorrelated amplitude and frequency variation should be a common phenomenon in pulsating stars that show harmonics in their periodograms, not only for the single-mode ones, but also for the multimode ones.

What are the origins of these uncorrelated variations? It could come from the fundamental pulsation mode or from the factors outside it. If we assume it comes from the fundamental mode, the physical origin might be the highly nonlinear interactions between the high-order harmonics in the outer layers (e.g., the dynamical interaction between a multishock structure and an outflowing wind in the coronal structure; Chadid et al. 2014). If we assume it comes from the factors beyond the fundamental mode, it could be caused by the perturbations from the hidden high-order p modes in the outer layers. Of course, these uncorrelated variations could be the results of a combination of these factors.

Another aspect of interest: what is the timescale of the uncorrelated variation? A relatively definite timescale would tell us which physical process it closely related to, and a stochastic timescale could be caused by some stochastic mechanisms and related to the stochastic excited modes. This issue should be studied in depth in future based on the accumulation of the high-precision time-series photometric data, which could shed light on some hidden corners of asteroseismology.

J.S.N. acknowledges support from the National Natural Science Foundation of China (NSFC; No. 12005124 and No. 12147215). H.F.X. acknowledges support from the Scientific and Technological Innovation Programs of Higher Education Institutions in Shanxi (STIP; No. 2020L0528) and the Applied Basic Research Programs of Natural Science Foundation of Shanxi Province (No. 202103021223320).

All the TESS data used in this paper can be found in MAST:10.17909/t9-nmc8-f686.

Software: Astropy (Astropy Collaboration et al. 2022).

ORCID iDs

Jia-Shu Niu (牛家树) <https://orcid.org/0000-0001-5232-9500>

Hui-Fang Xue (薛会芳) <https://orcid.org/0000-0001-6027-4562>

References

- Aerts, C. 2021, *RvMP*, **93**, 015001
 Alton, K. B. 2019, *JAAVSO*, **47**, 231
 Alton, K. B. 2022a, *RMxAA*, **58**, 109
 Alton, K. B. 2022b, *OEJV*, **223**, 1
 Astropy Collaboration, Price-Whelan, A. M., Lim, P. L., et al. 2022, *ApJ*, **935**, 167
 Blake, R. M., Delaney, P., Khosravani, H., Tome, J., & Lightman, M. 2003, *PASP*, **115**, 212
 Bowman, D. M., Hermans, J., Daszyńska-Daszkiewicz, J., et al. 2021, *MNRAS*, **504**, 4039
 Breger, M. 2000, in ASP Conf. Ser. 210, Delta Scuti and Related Stars, ed. M. Breger & M. Montgomery (San Francisco, CA: ASP), 3
 Breger, M., & Montgomery, M. H. 2014, *ApJ*, **783**, 89
 Brickhill, A. J. 1992, *MNRAS*, **259**, 519
 Cerasiki, W. 1904, *AN*, **165**, 61
 Chadid, M., Vernin, J., Preston, G., et al. 2014, *AJ*, **148**, 88
 Csörnyei, G., Szabados, L., Molnár, L., et al. 2022, *MNRAS*, **511**, 2125
 Daszyńska-Daszkiewicz, J., Walczak, P., Pamiatnykh, A. A., & Szewczuk, W. 2022, *MNRAS*, **512**, 3551
 Degroote, P., Briquet, M., Catala, C., et al. 2009, *A&A*, **506**, 111
 Handler, G. 2009, in AIP Conf. Ser. 1170, Stellar Pulsation: Challenges for Theory and Observation, ed. J. A. Guzik & P. A. Bradley (Melville, NY: AIP), 403
 Handler, G., Pikall, H., & Diethelm, R. 1998, *IBVS*, **4549**, 1
 Hintz, E. G., & Joner, M. D. 1997, *PASP*, **109**, 639
 Holdsworth, D. L., Smalley, B., Gillon, M., et al. 2014, *MNRAS*, **439**, 2078
 Jenkins, J. M., Twicken, J. D., McCauliff, S., et al. 2016, *Proc. SPIE*, **9913**, 99133E
 Joner, M. D. 1982, *PASP*, **94**, 289
 Kazarovets, E. V., Samus, N. N., Durlevich, O. V., et al. 2020, *PZ*, **40**, 6
 Khruslov, A. V. 2014, *PZP*, **14**, 1
 Khruslov, A. V. 2022, *OAst*, **31**, 148
 Kiss, L. L., & Derekas, A. 2000, *IBVS*, **4950**, 1
 Kurtz, D. W., Bowman, D. M., Ebo, S. J., et al. 2016, *MNRAS*, **455**, 1237
 Kurtz, D. W., Shibahashi, H., Murphy, S. J., Bedding, T. R., & Bowman, D. M. 2015, *MNRAS*, **450**, 3015
 Li, L. J., Qian, S. B., & Zhu, L. Y. 2018, *ApJ*, **863**, 151
 McNamara, D. H., & Feltz, K. A. J. 1980, *PASP*, **92**, 195
 Montgomery, M. H., & Odonoghue, D. 1999, *DSSN*, **13**, 28
 Mow, B., Reinhart, E., Nhim, S., & Watkins, R. 2016, *AJ*, **152**, 17
 Nijland, A. A. 1923, *Utrecht Rech. Astr.*, **8**, 144
 Niu, J.-S., Fu, J.-N., Li, Y., et al. 2017, *MNRAS*, **467**, 3122
 Niu, J.-S., Fu, J.-N., & Zong, W.-K. 2013, *RAA*, **13**, 1181
 Niu, J.-S., & Xue, H.-F. 2022, *ApJL*, **938**, L20
 Pápics, P. I., Tkachenko, A., Van Reeth, T., et al. 2017, *A&A*, **598**, A74
 Poleski, R., Soszyński, I., Udalski, A., et al. 2010, *AcA*, **60**, 1
 Poretti, E., Rainer, M., Weiss, W. W., et al. 2011, *A&A*, **528**, A147
 Rathour, R. S., Smolec, R., & Netzel, H. 2021, *MNRAS*, **505**, 5412
 Ricker, G. R., Winn, J. N., Vanderspek, R., et al. 2015, *JATIS*, **1**, 014003
 Szeidl, B., & Mahdy, H. A. 1981, *CoKon*, **75**, 1
 Uytterhoeven, K., Moya, A., Grigahcène, A., et al. 2011, *A&A*, **534**, A125
 VanderPlas, J. T. 2018, *ApJS*, **236**, 16
 Wils, P., Rozakis, I., Kleidis, S., Hambach, F. J., & Bernhard, K. 2008, *A&A*, **478**, 865
 Wu, Y. 2001, *MNRAS*, **323**, 248
 Xue, H.-F., Fu, J.-N., Fox-Machado, L., et al. 2018, *ApJ*, **861**, 96
 Xue, H.-F., & Niu, J.-S. 2020, *ApJ*, **904**, 5
 Xue, H.-F., Niu, J.-S., & Fu, J.-N. 2022, *RAA*, **22**, 105006
 Yacob, A. M., Berdnikov, L. N., Pastukhova, E. N., Kniazev, A. Y., & Whitelock, P. A. 2022, *MNRAS*, **516**, 2095
 Yang, T.-Z., Zuo, Z.-Y., Li, G., et al. 2021, *A&A*, **655**, A63
 Yang, X. H., Fu, J. N., & Zha, Q. 2012, *AJ*, **144**, 92
 Zhou, A.-Y., Jiang, S.-Y., Chayan, B., & Du, B.-T. 2002, *Ap&SS*, **281**, 699
 Zong, W., Charpinet, S., Fu, J.-N., et al. 2018, *ApJ*, **853**, 98